2005 American Control Conference
June 8-10, 2005. Portland, OR, USA



# Control Design Implementation for Sawyer Motors Used in Manufacturing Systems

P. Krishnamurthy, F. Khorrami, T.L. Ng, and I. Cherepinsky

*Abstract*— **In this paper, hardware integration and control design for a dual-axis linear stepper (Sawyer) motor are addressed. In particular, the Sawyer motor used in the Yaskawa/MotoMan manufacturing system which is utilized in various applications such as assembly, packaging, sorting, and probing, is considered. These motors are equipped with four optical sensors with a position resolution of 0.25 microns. We develop a detailed model of the motor for control validation and provide a comparison of two control designs, namely, a PD (or PID) and a robust adaptive nonlinear controller. To achieve high performance, a number of practical issues (such as delay/latency, finite sampling time, sensor noise, commutation rate, etc.) need to be considered. Effects of these factors are outlined and experimentally demonstrated. Both the considered controllers utilize knowledge of motor position and velocity in all axes. Current measurements are not required. Either numerical differentiation or a dynamic observer can be used to construct the velocity signals from the measured position data. The designed nonlinear controller provides practical stabilization of position tracking errors and achieves better overall performance. Adaptations are utilized so that no knowledge of the electromechanical system parameters is required. The proposed nonlinear controller is robust to load torques, friction, cogging forces, and other disturbances satisfying certain bounds. Furthermore, the controller corrects for the unintended yaw and achieves synchrony of the motor and rotor teeth. We have also observed that if the rotational motion is not corrected for, the performance is very poor for both controllers. This is also true in the case of delay/latency and higher rates of commutation.**

## I. INTRODUCTION

Sawyer motors are dual-axis linear motion motors widely used in wafer probing applications and in automated assembly. These motors are capable of high position resolution (2 $\mu m$ with open-loop microstepping control), rapid acceleration ($20m/sec^2$), and high speed moves ($1.5m/sec$) with low mass payloads. On the other hand, primarily because they are operated as open-loop stepper motors, they can miss steps, have long settle times of 100-200 msec, have low disturbance rejection (stiffness of 1,000 lb/inch), and fall short of their potential capabilities due to possible loss of synchrony between motor and platen teeth.

The Sawyer motor consists of a housing in which four forcers (or forcer-pairs) are symmetrically mounted (two for each direction of motion, Figure 1). The motor operates on a steel waffle platen and is floated on the platen by an air bearing (at a nominal height of 20 microns) so that stiction is eliminated. The aforementioned design of these motors eliminates the need for lead screws, belts, and pulleys, adding to their mechanical simplicity of design. The linear motion is achieved through application of a proper sequence of phase currents. The motor has two translational degrees of freedom along with an unwanted rotational degree of freedom[1] (yaw) due to the fact that not all forcers can be mounted at the center of mass. Yawing of the motor is caused by asymmetries in the forcers and leads to loss of synchrony between motor and platen teeth resulting in severe drop of generated electromagnetic force. In this paper, we will address a number of issues in control design (i.e., delay, yaw correction, feedforward control, etc.) that must be considered to achieve a high performance.

The problem of closed-loop control for this type of stepper motors has received attention in the literature [1,2]. An adaptive variable structure controller is proposed in [3] while a hybrid control strategy is developed in [4]. A PID controller with a velocity estimator is investigated in [5]. A controller which uses only motor position and yaw angle measurements is presented in [6]. Though the electrical dynamics are faster than the mechanical dynamics, the performance improvement attained by including the current dynamics in the closed-loop has been clearly demonstrated for other types of stepper motors [7,8]. Recent results which incorporate the electrical dynamics include [9–12] for permanent magnet stepper motors and [13,14] for variable reluctance stepper motors. Motivated by this consideration, a detailed model for the overall dynamics of the voltage-fed Sawyer motor including the electrical dynamics was obtained in [15] and this model was used for control design without, however, requiring current measurements. A multivariable generalization of the popular two-phase (one position variable) Direct-Quadrature (D-Q) transformation [16] to the Sawyer motor which has eight current phases and three position states was developed in [15] to transform the fourteenth order Sawyer motor dynamics into three third-order subsystems along with a fifth-order appended dynamics. The performance improvement attained by including consideration of current dynamics in control design was demonstrated via simulations in [15].

In this paper, we demonstrate using experimental results that the robust adaptive controllers developed in [1–3,6,15] provide performance improvement over PD/PID based controllers. Noting that PD/PID controllers themselves provide considerable performance improvement over open-loop microstepping [5], it is seen that the improvement over open-loop microstepping (which is still the most commonly used technique in industrial applications) obtained by using the robust adaptive controller is significant. The experimental

This work is supported in part by the NSF under grant ECS-9977693.

The first three authors are with the Control/Robotics Research Laboratory(CRRL), Dept. of Electrical and Computer Engineering, Polytechnic University, Six Metrotech Center, Brooklyn, New York 11201. The last author is with Sikorsky in Stratford, CT.
Emails: pk@crrl.poly.edu, khorrami@smart.poly.edu, tlng@crrl.poly.edu, igor@crrl.poly.edu.

[1]Alternatively, one may use this rotational motion as an additional degree of freedom with a range of a few degrees.

setup and the custom hardware built to interface with the position sensors and the real-time processing computer are described in Section II. The mathematical model of the Sawyer motor is briefly summarized in Section III. The commutation technique to convert force and torque commands into current commands is explained in Section IV along with the technique used to compensate for the closed-loop delay. Delay compensation in commutation is vital for this type of motor to operate at the peak of the force and torque curves. The robust adaptive nonlinear controller is developed in Section V. Experimental results obtained with the adaptive controller are presented in Section VI and compared with results obtained with a PD controller.

## II. Experimental Setup and Hardware Development

The objective of this paper is to improve the performance of the Yaskawa/MotoMan manufacturing cell (refer to Figure 3) by enhancing the performance of the two-phase Sawyer motor used in this system. The motor has the typical construction of a Sawyer motor as described earlier and is provided with four optical position sensors (with resolutions of 0.25 $\mu m$, i.e., 12-bits) attached to the motor housing. A typical plot of sensor data showing the jitter (i.e., sensor noise) in the measured position is given in Figure 4. Two sensors on opposite sides of the puck pick up motor position in each translational direction. The two opposite sensors can be used to calculate the rotation of the puck relative to the platen; therefore, allowing control of the in-plane (yaw) rotation of the motor. The sensor outputs are transmitted along the umbilical back to the main processor using a serial format after boosting the signal levels.

Since the motor is part of a larger manufacturing system with many other features, we needed to build the appropriate interfaces to couple the motor to our real-time processing computer based on the DSpace dual Alpha/C40 combination with our own custom designed I/O boards integrated with the DSpace PHS bus. The custom designed I/O board accepts fiber optic inputs and outputs using synchronous serial communications. Therefore, we needed to develop an interface to convert position sensor data transmitted

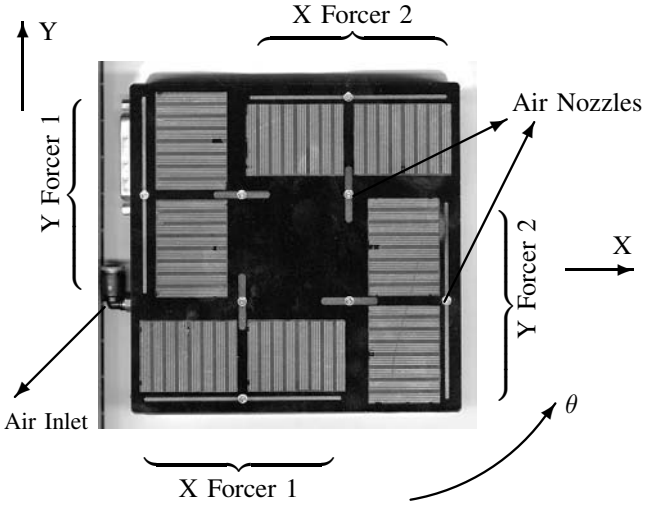


Fig. 1. Bottom view of a two-phase Sawyer motor (model XY1304 from Normag, Inc.).

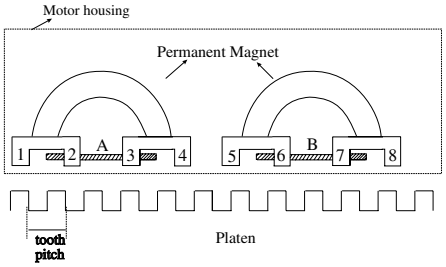


Fig. 2. A two-phase forcer pair.

Fig. 3. Motoman/ Yaskawa manufacturing system.

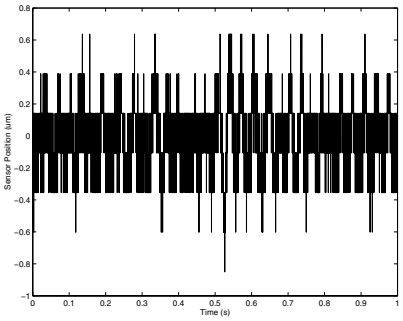


Fig. 4. Position jitter from optical sensors.

from the DSP chip internal to the motor to the serial format used by our custom designed board. This interface board is mounted on the motor and includes a Xilinx FPGA chip and the serial communication decoders and the fiber optic interface. The fiber carrying all the four position data plugs into our custom designed I/O board. Since the communication from the sensors to our sensor board on the motor is asynchronous and the transmission of this signal to our custom designed I/O board and to the real-time control computer is synchronous, a variable latency is created in attaining the position data in the real-time processor. This variable latency is in the range of 70 to 90 micro-seconds. In addition, the optical sensors can output sensor positions at a rate of about 5KHz thus producing an additional 200 micro-second latency/delay. There are also delays corresponding to instruction cycles performing 2 reads and 4 writes (reading in sensor data and outputting voltage commands to the coils) and due to the amplifier and other component bandwidth. This latency is very important to be modelled in the motor commutation to achieve reasonable closed-loop performance.

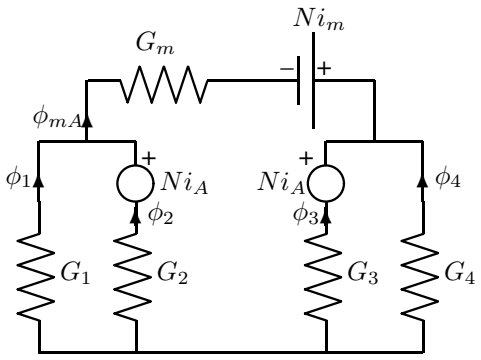


Fig. 5. Equivalent circuit of one phase.

The voltage command outputs to the eight motor coils are transmitted out via our custom designed I/O board through fibers to the dedicated boards built by us to process the serial data and to provide the proper commutation to the digital/analog converters internal to the motor amplifiers (hence bypassing the internal commutations built into the amplifiers). This interface is done via fiber optic cable to properly isolate the computer from the amplifiers. The overall hardware has been thoroughly tested and all latencies have been measured. However, the latencies being variable can not be known ahead of time. Hence, for control design, we have used an average latency for the overall system.

## III. Modeling

Figure 2 depicts a two-phase forcer pair whose equivalent magnetic circuit for one phase is shown in Figure 5. A similar circuit can be drawn for the other phase of the forcer which is energized by winding B. Here, the permanent magnet is modeled by the constant mmf source $Ni_m$ in series with permeance $G_m$. $N$ is the number of turns in the windings. Solving the circuit in Figure 5 results in the following expressions [17,3,8] for $\phi_A = \phi_2 + \phi_3$ and $\phi_{mA}$:

$$\begin{aligned}\phi_A &= \frac{Ni_A}{G_1+G_2}\left[\frac{G_m(G_1-G_2)^2}{G_1+G_2+2G_m}+2G_1G_2\right] \\ &\quad + \frac{G_m(G_2-G_1)}{G_1+G_2+2G_m}Ni_m \\ \phi_{mA} &= \frac{G_mN}{G_1+G_2+2G_m}\left[(G_2-G_1)i_A+(G_1+G_2)i_m\right] \quad (1)\end{aligned}$$

where $G_i, i = 1,\ldots,8$ is the permeance of the airgap under the $i^{th}$ tooth (see Figure 2), $i_A$ is the current in winding $A$, $\phi_A$ is the flux associated with the winding $A$, and $\phi_{mA}$ is the total flux associated with the permanent magnet corresponding to phase $A$. Similar expressions can be worked out for $\phi_{mB}$ and $\phi_B$ associated with the second phase of the forcer. These expressions will involve permeances $G_5,\ldots,G_8$. From the geometry of the teeth, $G_1(x) = G_3(x), G_5(x) = G_7(x), G_2(x) = G_4(x) = G_1(x-\frac{p}{2}), G_6(x) = G_8(x) = G_5(x-\frac{p}{2}) = G_1(x+\frac{p}{4})$ where $(x,y)$ is the position of the motor on the platen. Furthermore, we assume that the permeances can be modeled as sinusoidal functions of the position, i.e., $G_1(x) = G_0 - G_a\sin(\gamma x)$ where $G_0$ and $G_a$ are positive constants ($G_0 \geq G_a$). $\gamma = \frac{2\pi}{p}$ where $p$ is the toothpitch. Using (1), we derive

$$\begin{aligned}\phi_A &= \left[\frac{NG_mG_a^2\sin^2(\gamma x)}{G_0(G_0+G_m)}+\frac{N(G_0^2-G_a^2\sin^2(\gamma x))}{G_0}\right]i_A \\ &\quad + \frac{NG_mG_a\sin(\gamma x)}{G_0+G_m}i_m \\ \phi_{mA} &= \frac{G_mN}{G_0+G_m}\left[G_a\sin(\gamma x)i_A + G_0i_m\right]\end{aligned}$$

$$\begin{aligned}\phi_B &= \left[\frac{NG_mG_a^2\cos^2(\gamma x)}{G_0(G_0+G_m)}+\frac{N(G_0^2-G_a^2\cos^2(\gamma x)}{G_0}\right]i_B \\ &\quad - \frac{NG_mG_a\cos(\gamma x)}{G_0+G_m}i_m \\ \phi_{mB} &= \frac{G_mN}{G_0+G_m}\left[-G_a\cos(\gamma x)i_B + G_0i_m\right]. \quad (2)\end{aligned}$$

These equations can be collected in matrix form as $N\phi = Li$ where $\phi = [\phi_A,\phi_B,\phi_{mA},\phi_{mB}]^T$, $i = [i_A,i_B,i_m,i_m]^T$, and $L$ is a $4\times4$ inductance matrix. The force ($F = \frac{1}{2}i^T\frac{\partial L}{\partial x}i$) generated by the forcer can be derived as

$$\begin{aligned}F &= \frac{1}{2}\left[\frac{\gamma N^2G_a^2\sin(2\gamma x)}{G_0+G_m}(i_B^2-i_A^2)\right. \\ &\quad \left.+\frac{2N^2\gamma G_mG_ai_m}{G_0+G_m}(i_A\cos(\gamma x)+i_B\sin(\gamma x))\right] \\ &\approx \kappa[i_A\cos(\gamma x)+i_B\sin(\gamma x)] \quad (3)\end{aligned}$$

where $\kappa = \gamma N^2G_ai_m$ is the force constant. The last step in (3) follows under the physically meaningful assumption $G_m >> G_0$ (i.e., the permeance of the iron path is much larger than the airgap permeance). Utilizing the same assumption, the electrical dynamics can be derived as

$$\begin{aligned}\dot{i}_A &= \frac{1}{N^2G_0}(v_A - i_AR_A - N^2\gamma G_ai_m\cos(\gamma x)\dot{x}) \\ \dot{i}_B &= \frac{1}{N^2G_0}(v_B - i_BR_B - N^2\gamma G_ai_m\sin(\gamma x)\dot{x}) \quad (4)\end{aligned}$$

where $v_A$ and $R_A$ denote the applied voltage and the resistance of winding $A$, respectively. To account for the yaw rotation of the motor housing, $x$ in (3) and (4) must be replaced by $x_1 = x + r\sin\theta$ where $\theta$ is the yaw rotation and $r$ is the distance from the center of the motor to the forcer.

Similar expressions can be derived for the second X-axis forcer with windings $(C,D)$ and for the two Y-axis forcers with windings $(E,F)$ and $(G,H)$. Denoting the forces generated by the two X-axis forcers by $F_{x1}$ and $F_{x2}$ and the forces generated by the two Y-axis forcers by $F_{y1}$ and $F_{y2}$, the total forces in X and Y directions and the torque are

$$\begin{aligned}F_x &= F_{x1}+F_{x2} \\ &= \kappa\{[i_A\cos(\gamma x_1)+i_B\sin(\gamma x_1)] \\ &\quad +[i_C\cos(\gamma x_2)+i_D\sin(\gamma x_2)]\} \quad (5) \\ F_y &= F_{y1}+F_{y2} \\ &= \kappa\{[i_E\cos(\gamma y_1)+i_F\sin(\gamma y_1)] \\ &\quad +[i_G\cos(\gamma y_2)+i_H\sin(\gamma y_2)]\} \quad (6) \\ \tau &= (F_{x1}-F_{x2})r+(F_{y1}-F_{y2})r \\ &= \kappa r\{[i_A\cos(\gamma x_1)+i_B\sin(\gamma x_1)] \\ &\quad -[i_C\cos(\gamma x_2)+i_D\sin(\gamma x_2)] \\ &\quad +[i_E\cos(\gamma y_1)+i_F\sin(\gamma y_1)] \\ &\quad -[i_G\cos(\gamma y_2)+i_H\sin(\gamma y_2)]\}. \quad (7)\end{aligned}$$

## IV. Commutation and Delay Compensation

A control law design considering the mechanical dynamics prescribes forces in the X and Y directions and the torque. The generated control values are commutated into the actual control inputs which are the voltages (or the currents if the electrical dynamics are considered fast) using the following commutation scheme which is derived from

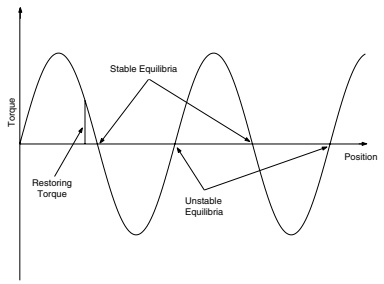


Fig. 6. Generated torque.

the force and torque expressions (5)-(7):

$$i_A = (\frac{F_x}{2\kappa} + \frac{\tau}{4\kappa r})\cos(\gamma x_1), i_B = (\frac{F_x}{2\kappa} + \frac{\tau}{4\kappa r})\sin(\gamma x_1)$$
$$i_C = (\frac{F_x}{2\kappa} - \frac{\tau}{4\kappa r})\cos(\gamma x_2), i_D = (\frac{F_x}{2\kappa} - \frac{\tau}{4\kappa r})\sin(\gamma x_2)$$
$$i_E = (\frac{F_y}{2\kappa} + \frac{\tau}{4\kappa r})\cos(\gamma y_1), i_F = (\frac{F_y}{2\kappa} + \frac{\tau}{4\kappa r})\sin(\gamma y_1)$$
$$i_G = (\frac{F_y}{2\kappa} - \frac{\tau}{4\kappa r})\cos(\gamma y_2), i_H = (\frac{F_y}{2\kappa} - \frac{\tau}{4\kappa r})\sin(\gamma y_2). \quad (8)$$

As mentioned in Section II, the closed-loop system contains a variable delay. Compensating for the delay in commutation is crucial in achieving high velocities since the generated forces and torques drop off rapidly if the errors between the actual positions and the positions used in the commutation law (8) are large. The reduction of the generated forces and torques is proportional to the cosine of the position error (see Figure 6). To compensate for the delay $\delta$, we need to essentially invert the delay transfer function $e^{-s\delta}$ using $e^{s\delta} \approx 1 + s\delta$ so that if the measured position of forcer 1 is $\hat{x}_1$, the estimated position is computed as $x_1 = \hat{x}_1 + \delta\dot{\hat{x}}_1$ and similarly for positions of other forcers.

## V. Robust Adaptive Controller

The dynamics of the Sawyer motor can be considered to be comprised of three coupled subsystems governing the X-axis, Y-axis, and yaw motions. The coupling between these subsystems is primarily in the current dynamics and the force and torque expressions. The X-axis subsystem dynamics are of the form

$$\dot{x} \;=\; x_v \;;\; \dot{x}_v \;=\; \frac{1}{M}(F_x - \eta x_v + F_{xd}) \quad (9)$$

where $x$ is the X-axis position of the center of the puck (i.e., $x = \frac{x_1+x_2}{2}$), $x_v$ is the X-axis velocity of the center of the puck, $\eta$ is the coefficient of viscous friction, and $F_{xd}$ is the force due to load, cogging, disturbances, etc., which can be assumed to be bounded affinely in positions and velocities. The Y-axis and yaw dynamics are analogous to (9).

In this section, a current-level robust adaptive controller is designed using backstepping to make $x$ and $y$ track given reference trajectories $x_{ref}$ and $y_{ref}$ while regulating yaw rotation to zero. No knowledge of motor electromechanical parameters is required. Only the geometrical parameters $r$ and $\gamma$ (i.e., the motor physical dimensions and the tooth-pitch) of the motor are assumed to be known. The designed controller incorporates adaptations to counter uncertainty in electromechanical parameters. The controller utilizes knowledge of motor position and velocity in all axes. Hence, the velocity signals must be constructed from measured position data using either numerical differentiation (with a low pass filter to reduce noise) or an observer [6,8]. The control design for the X-axis subsystem is described below. The design for the Y-axis controller is similar. A PD controller usually suffices for the yaw subsystem since rotations are small with the yaw reference being zero.

The backstepping-based controller design starts with the introduction of a Lyapunov function $V_{x1} = (1/2)(x - x_{ref})^2$. Differentiating $V_{x1}$, we obtain $\dot{V}_{x1} = (x - x_{ref})(x_v - \dot{x}_{ref})$. If $x_v$ were the actual control input, $\dot{V}_{x1}$ could be rendered nonpositive by choosing $x_v = x_v^* = \dot{x}_{ref} - k_1(x - x_{ref})$ with a constant $k_1 \geq 0$. However, since $x_v$ is not the actual control input, the *virtual* control law $x_v^*$ must be *stepped back* to the actual control inputs (the currents) using a step of backstepping with the Lyapunov function $V_{x2} = (1/2)(x - x_{ref})^2 + [M/(2c_2\kappa)](x_v - x_v^*)^2$ with a constant $c_2 > 0$. Differentiating $V_{x2}$,

$$\begin{aligned}\dot{V}_{x2} \;=\; & -k_1(x-x_{ref})^2 + \frac{1}{c_2}(x_v - x_v^*)\Big[\hat{F}_x + c_2(x - x_{ref}) \\ & -\frac{\eta}{\kappa}(x_v - x_v^*) + \frac{1}{\kappa}F_{xd} \\ & -\frac{M}{\kappa}\Big(\ddot{x}_{ref} - k_1(x_v - \dot{x}_{ref})\Big) - \frac{\eta}{\kappa}x_v^*\Big] \end{aligned} \quad (10)$$

where the *scaled force* $\hat{F}_x$ is given by $\hat{F}_x = \frac{F_x}{\kappa}$. Note that $\hat{F}_x$ is a function of $i_A, \ldots, i_D$ and does not involve any unknown parameters. At this point, adaptations $\alpha_1$ and $\alpha_2$ are introduced to compensate for the unknown parameters $M/\kappa$ and $\eta/\kappa$ that appear in (10). These adaptations provide an adaptive feedforward term and adaptive friction compensation. Since the same unknown parameters occur in the Y-axis controller design, a composite Lyapunov function can be utilized to avoid separate adaptations in the X-axis and Y-axis controllers, thereby reducing the overall controller dynamic order. Hence, defining $V_2 = V_{x2} + V_{y2}$ where $V_{y2}$ is defined analogous to $V_{x2}$, we have

$$\begin{aligned}\dot{V}_2 \;=\; & -k_1(x - x_{ref})^2 - k_1(y - y_{ref})^2 \\ & +\frac{1}{c_2}(x_v - x_v^*)\Big[\hat{F}_x + c_2(x - x_{ref}) - \frac{\eta}{\kappa}(x_v - x_v^*) \\ & -\alpha_1\Big(\ddot{x}_{ref} - k_1(x_v - \dot{x}_{ref})\Big) - \alpha_2 x_v^* + \frac{1}{\kappa}F_{xd}\Big] \\ & +\frac{1}{c_2}(y_v - y_v^*)\Big[\hat{F}_y + c_2(y - y_{ref}) - \frac{\eta}{\kappa}(y_v - y_v^*) \\ & -\alpha_1\Big(\ddot{y}_{ref} - k_1(y_v - \dot{y}_{ref})\Big) - \alpha_2 y_v^* + \frac{1}{\kappa}F_{yd}\Big] \\ & -\frac{1}{c_2}\Big(\frac{M}{\kappa} - \alpha_1\Big)\Big((x_v - x_v^*)[\ddot{x}_{ref} - k_1(x_v - \dot{x}_{ref})] \\ & +(y_v - y_v^*)[\ddot{y}_{ref} - k_1(y_v - \dot{y}_{ref})]\Big) \\ & -\frac{1}{c_2}\Big(\frac{\eta}{\kappa} - \alpha_2\Big)\Big((x_v - x_v^*)x_v^* + (y_v - y_v^*)y_v^*\Big). \end{aligned} \quad (11)$$

Designing the scaled forces $\hat{F}_x$ and $\hat{F}_y$ as

$$\begin{aligned}\hat{F}_x \;=\; & -c_2(x - x_{ref}) - k_2(\dot{x} - x_v^*) \\ & +\alpha_1[\ddot{x}_{ref} - k_1(\dot{x} - \dot{x}_{ref})] + \alpha_2 x_v^* \end{aligned} \quad (12)$$

$$\begin{aligned}\hat{F}_y \;=\; & -c_2(y - y_{ref}) - k_2(\dot{y} - y_v^*) \\ & +\alpha_1[\ddot{y}_{ref} - k_1(\dot{y} - \dot{y}_{ref})] + \alpha_2 y_v^* \end{aligned} \quad (13)$$

with $k_2$ being a positive constant and the parameter adaptation dynamics as

$$\begin{aligned}\dot{\alpha}_1 \;=\; & -\sigma_{\alpha_1}\alpha_1 - c_{\alpha_1}\Big\{(\dot{x} - x_v^*)[\ddot{x}_{ref} - k_1(\dot{x} - \dot{x}_{ref})] \\ & +(\dot{y} - y_v^*)[\ddot{y}_{ref} - k_1(\dot{y} - \dot{y}_{ref})]\Big\} \end{aligned} \quad (14)$$

$$\dot{\alpha}_2 \;=\; -\sigma_{\alpha_2}\alpha_2 - c_{\alpha_2}\Big\{(\dot{x} - x_v^*)x_v^* + (\dot{y} - y_v^*)y_v^*\Big\} \quad (15)$$

where $c_{\alpha_1}$ and $c_{\alpha_2}$ are positive constants and $\sigma_{\alpha_1}$ and $\sigma_{\alpha_2}$ are nonnegative constants (which provide $\sigma$-modification to prevent parameter drift instability), closed-loop stability and practical tracking can be demonstrated using the augmented Lyapunov function

$$V = V_2 + \frac{1}{2c_{\alpha_1}c_2}(\alpha_1 - \frac{M}{\kappa})^2 + \frac{1}{2c_{\alpha_2}c_2}(\alpha_2 - \frac{\eta}{\kappa})^2 \quad (16)$$

which yields, after certain manipulations and bounding, $\dot{V} \leq -\epsilon_1 V + \epsilon_2$, with $\epsilon_1$ and $\epsilon_2$ being bounded. The detailed stability proof is omitted here for brevity and can be constructed along similar lines as in our previous papers [1–3,6,15] and recent book [8] which also provide more general control designs which take into account additional physical perturbations and effects. To improve the performance of the designed controller further, separate parameter estimates can be used for the $X$ and $Y$ axes and the rotation $\theta$. The adaptive nonlinear controller designed in this section and its implementation are summarized below.

*Summary of controller design:* Given reference trajectories $x_{ref}$ and $y_{ref}$ to be tracked in the $X$ and $Y$ directions, the control design procedure is summarized as follows:

1) Pick positive constants $k_{p\theta}$, $k_{d\theta}$, $k_2$, $c_2$, $c_{\alpha_1}$, and $c_{\alpha_2}$. Pick nonnegative constants $k_1$, $\sigma_{\alpha_1}$, and $\sigma_{\alpha_2}$.
2) Utilize the delay compensation scheme in Section IV to obtain position estimates $x_1, x_2, x_3, x_4$ of the four forcers. The average positions and the rotation are computed as $x = (x_1 + x_2)/2$, $y = (y_1 + y_2)/2$, and $\theta = [(x_1 - x_2) + (y_2 - y_1)]/4r$.
3) Obtain velocity estimates using either the observer design technique in [6] or a numerical differentiation (with a low pass filter to reduce noise).
4) Implement the adaptation dynamics shown in (14) and (15) with
$$\begin{aligned} x_v^* &= \dot{x}_{ref} - k_1(x - x_{ref}) \\ y_v^* &= \dot{y}_{ref} - k_1(y - y_{ref}). \end{aligned} \quad (17)$$
5) Compute $\hat{F}_x$ and $\hat{F}_y$ as shown in (12) and (13). Also, compute $\hat{\tau} = -k_{p\theta}\theta - k_{d\theta}\dot{\theta}$.
6) Calculate the currents using the commutation law given in (8) with $F_x/\kappa$ and $\tau/\kappa$ replaced with $\hat{F}_x$ and $\hat{\tau}$, respectively, i.e., $i_A = (\frac{\hat{F}_x}{2} + \frac{\hat{\tau}}{4r})\cos(\gamma x_1)$, etc.

The adaptive nonlinear controller is compared in Section VI with a PD controller of the form

$$\begin{aligned} \hat{F}_x &= -k_p(x - x_{ref}) - k_d(\dot{x} - \dot{x}_{ref}) \\ \hat{F}_y &= -k_p(y - y_{ref}) - k_d(\dot{y} - \dot{y}_{ref}) \\ \hat{\tau} &= -k_{p\theta}\theta - k_{d\theta}\dot{\theta} \end{aligned} \quad (18)$$

with $k_p, k_d, k_{p\theta}$, and $k_{d\theta}$ being positive gains. The currents are computed as in Step (6) above.

## VI. Experimental Results

To demonstrate the efficacy of the proposed control designs, both controllers have been implemented on our experimental testbed. The following important observations need to be pointed out before comparing the results:

1) If the motor rotation is not compensated for, the motor would lose synchrony and stall (i.e., rotate off alignment).
2) Having compensated for motor rotation, without accomodating for the latency in position measurement, the motor would not be able to attain high velocities (since the generated forces are much smaller than is possible).
3) Having compensated for the latency and motor rotation, the highest speed and acceleration could not be achieved at lower commutation rates. Since the position sensor measurements are updated at a rate of about 5KHz, we have commutated the currents in the amplifiers at a higher rate of 20KHz. This allowed us to achieve higher speeds and accelerations for the motor.
4) Having compensated for the effects of motor yawing, latency/delay, and commutation rates, the controller gains are restricted to small values if step reference trajectories are used resulting in slow moves. Increasing the controller gains would saturate the actuators (since the errors are initially large with step reference trajectories) and result in loss of motor synchrony and poor performance. Hence, a smooth reference trajectory is used.

To summarize, it is essential that the motor controller does take into account effects of motor yawing, latency/delay, and commutation rates. Furthermore, compensating for these effects yields much higher forces and therefore speeds of the motor since the motor operates on the peak of the force-displacement curve.

A number of point-to-point maneuvers and trajectory tracking experiments have been performed. For brevity, we provide plots for a 20 cm move in one axis while correcting for rotations in both axes. Rather than a trapezodial velocity profile, a smooth velocity profile was provided as the reference trajectory in order to keep the jerk finite (rather than being infinite as in the case of trapezoidal velocity profile). To generate the reference trajectory (shown in Figure 7), we imposed a maximum acceleration of 12 $m/s^2$ and a maximum velocity of 1.1265 $m/s$. With these maximum velocity and acceleration limits, the total maneuver time is 0.325 $s$ for our smooth velocity trajectory.

The parameters of the adaptive nonlinear controller were picked to be $k_1 = 0$, $k_2 = 32$, $c_2 = 14000$, $c_{\alpha_1} = 100$, $c_{\alpha_2} = 10$, $k_{p\theta} = 100$, $k_{d\theta} = 2$, and $\sigma_{\alpha_1} = \sigma_{\alpha_2} = 0$. The parameters of the PD controller were picked to be $k_p = k_1k_2 + c_2 = 14000$, $k_d = k_2 = 32$, $k_{p\theta} = 100$, and $k_{d\theta} = 2$ so that the adaptive controller and the PD controller differ only in the adaptations. The experimental results from the motor using the PD controller is shown in Figure 8. The experimental results with the nonlinear adaptive controller are depicted in Figures 9 and 10.

It may be observed that the robust adaptive nonlinear controller performed better than the PD controller. The total move time (including settling time) with PD controller is 0.423 $s$ versus 0.357 $s$ with the adaptive controller (this corresponds to a percentage improvement of 18.5 %). The adaptive controller reduces the number of cycles to settle at the end of the move from 4 cycles to 1 cycle and achieves better steady state error (0.9 $\mu m$ versus 1.32 $\mu m$). Also, the RMS error during steady state is improved with the

adaptive controller (0.95 $\mu m$ versus 1.35 $\mu m$). The steady state error with either controller can be further reduced using an integral term. However, this would increase the settling time and slow down the move.

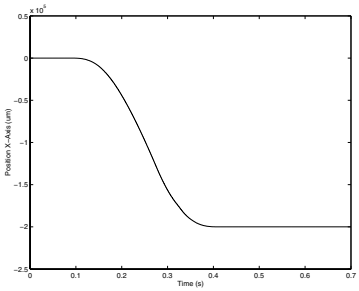


Fig. 7. Smooth position reference trajectory.

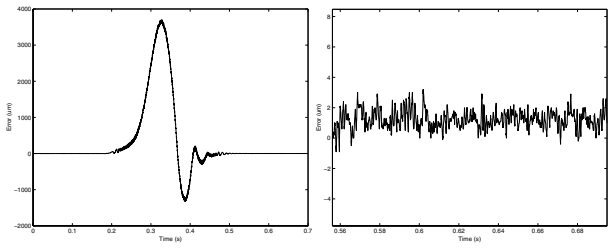


(a) (b)

Fig. 8. Motor performance using the PD controller: (a) Error ($\mu m$), (b) Error ($\mu m$) during steady state.

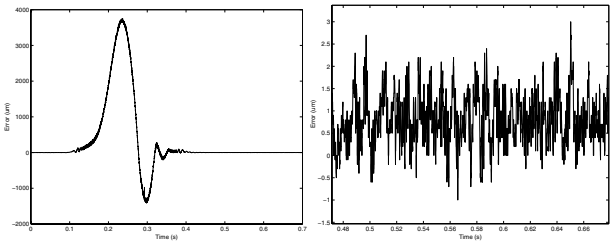


(a) (b)

Fig. 9. Motor performance using the adaptive nonlinear controller: (a) Error ($\mu m$), (b) Error ($\mu m$) during steady state.

## VII. Conclusion

A host of practical issues and two controller designs for Sawyer motors were reported and experimentally verified. The two controllers considered are a PD (or PID) and a robust adaptive nonlinear controller. Both controllers utilized position and velocity measurements. A detailed model of the motor incorporating the significant uncertainties and disturbances was considered. Our previous papers on adaptive nonlinear controllers for Sawyer motors had shown their superior performance compared to PD and PID controllers. In this paper, we have experimentally verified this on a motor setup. Adaptations are utilized to eliminate requirement of any knowledge of motor parameters. The proposed controller which has second-order dynamics provides asymptotic stabilization and is robust to load torques, friction, cogging forces, and other disturbances satisfying certain bounds. As part of this effort, a considerable amount of hardware development was performed.

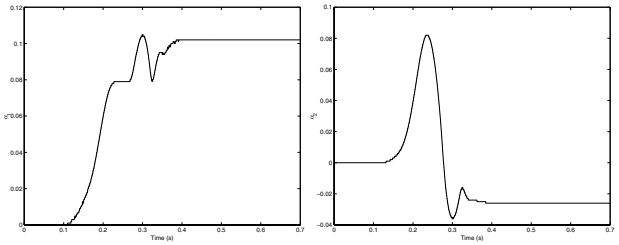


(a) (b)

Fig. 10. Motor performance using the adaptive nonlinear controller: (a) $\alpha_1$, (b) $\alpha_2$.

## References


[1] F. Khorrami, H. Melkote, and J. Ish-Shalom, "Advanced control system design for high speed ultra accurate manufacturing systems," in *Proceedings of the American Control Conf.*, Albuquerque, NM, June 1997, pp. 164–165.

[2] H. Melkote, F. Khorrami, and J. Ish-Shalom, "Closed-loop control of a three degree-of-freedom ultra accurate linear stepper motor," in *Proceedings of the IEEE Conf. on Control Applications*, Hartford, CT, Oct. 1997, pp. 639–644.

[3] H. Melkote and F. Khorrami, "Closed-loop control of a base xy stage with rotational degree-of-freedom for a high-speed ultra-accurate manufacturing system," in *Proceedings of the IEEE Int. Conf. on Robotics and Automation*, Detroit, MI, May 1999, pp. 1812–1817.

[4] A. E. Quaid and A. A. Rizzi, "Robust and efficient motion planning for a planar robot using hybrid control," in *Proceedings of the IEEE Int. Conf. on Robotics and Automation*, San Francisco, CA, Apr. 2000, pp. 4021–4026.

[5] A. E. Quaid and R. L. Hollis, "3-dof closed-loop control for planar linear motors," in *Proceedings of the IEEE Int. Conf. on Robotics and Automation*, Leuven, Belgium, May 1998, pp. 2488–2493.

[6] H. Melkote and F. Khorrami, "Output feedback control of a three degree-of-freedom linear stepper motor with position measurements only," in *Proceedings of the American Control Conf.*, San Diego, CA, June 1999, pp. 2531–2535.

[7] D. Dawson, J. Hu, and T. Burg, *Nonlinear Control of Electric Machinery*. New York: Marcel Dekker, Inc., 1998.

[8] F. Khorrami, P. Krishnamurthy, and H. Melkote, *Modeling and Adaptive Nonlinear Control of Electric Motors*. New York: Springer Verlag, 2003.

[9] R. C. Speagle, J. Hu, D. M. Dawson, and Z. Qu, "Robust tracking control of a permanent magnet stepper motor without current measurements," in *Proceedings of the IEEE Conf. on Control Applications*, Vancouver, Canada, Sep. 1993, pp. 153–158.

[10] T. Burg, J. Hu, D. M. Dawson, and P. Vedagarbha, "A global exponential position tracking controller for a permanent magnet stepper motor via output feedback," in *Proceedings of the IEEE Conf. on Control Applications*, Glasgow, UK, Aug. 1994, pp. 213–218.

[11] H. Melkote and F. Khorrami, "Robust nonlinear control and torque ripple reduction for permanent magnet stepper motors," *IEE Proceedings on Control Theory and Applications*, vol. 146, no. 2, pp. 186–196, March 1999.

[12] P. Krishnamurthy and F. Khorrami, "Robust adaptive voltage-fed permanent magnet step motor control without current measurements," *IEEE Transactions on Control Systems Technology*, vol. 11, no. 3, pp. 415–425, May 2003.

[13] J. Carroll and D. Dawson, "Adaptive tracking control of a switched reluctance motor turning an inertial load," in *Proceedings of the American Control Conf.*, San Francisco, CA, June 1993, pp. 670–674.

[14] H. Melkote, F. Khorrami, S. Jain, and M. Mattice, "Robust adaptive control of variable reluctance stepper motors," *IEEE Transactions on Control Systems Technology*, vol. 7, no. 2, pp. 212–221, Mar. 1999.

[15] P. Krishnamurthy and F. Khorrami, "Robust adaptive control of sawyer motors without current measurements," *IEEE Transactions on Mechatronics*, vol. 9, no. 4, pp. 689–696, Dec. 2004.

[16] R. H. Park, "Two-reaction theory of synchronous machines-generalized method of analysis," *AIEE Transactions*, no. 48, pp. 716–727, Nov. 1929.

[17] S. Nicholson, E. Burgett and A. Wallack, "Optical position sensing for closed loop control of linear stepper motors," in *Proceedings of the Int. Conf. of Advanced Mechatronics*, Tokyo, Japan, Aug. 1993.